Stationary and moving intrinsic localized modes in one-dimensional monatomic lattices with cubic and quartic anharmonicity

S. R. Bickham, S. A. Kiselev, and A. J. Sievers
Laboratory of Atomic and Solid State Physics and Materials Science Center, Cornell University, Ithaca, New York 14853-2501
(Received 11 January 1993)

By locally distorting a perfect one-dimensional lattice that contains a cubic and quartic nonlinearity in the nearest-neighbor potential, we demonstrate that self-localized vibrational modes are stable even for large cubic anharmonicities. Simulations are used to test the eigenvectors and eigenfrequencies of both stationary and moving localized modes. The frequency of the localized vibration decreases with increasing cubic anharmonicity until it approaches the maximum plane-wave frequency, where the mode becomes unstable. As the cubic anharmonicity increases, the eigenvector also becomes more localized until it resembles a triatomic molecule, beyond which the mode again becomes unstable. This study examines intrinsic localized modes over the complete range of possible anharmonicity and amplitude values.

I. INTRODUCTION

In recent years, several analytical[1-4] and simulation[5,6] studies of the dynamical properties of perfect lattice with hard quartic anharmonicity have shown the existence of intrinsic localized modes with frequencies above the maximum of the plane-wave spectrum. These modes typically involve sizable amplitudes on only a few lattice sites, and because they exist in perfect lattices, they may appear at any site due to translational symmetry.[7] One study has shown that lattices with positive quartic anharmonicity can support moving intrinsic localized modes that have group velocities up to 10% of the speed of sound in the lattice.[8] There have also been investigations of the long-term behavior[9] of intrinsic localized modes and their stability under infinitesimal perturbations of the eigenvector.[10]

The works mentioned above focus on lattices with only harmonic and positive quartic anharmonicity in the nearest-neighbor potential. Cubic anharmonicity has typically only been included when the nonlinearity is a small perturbation[11,12] or when the equations of motion are analyzed within the continuum approximation.[13,14] Recently, Burlakov and Kiselev[15] reported simulations of intrinsic localized modes in a nonlinear chain with cubic and quartic force constants, but because the correct eigenvector was not used only unstable modes were identified. Takeno and Hori[16] have also published an analytical study in which an approximate solution for stationary and moving intrinsic localized modes in a lattice with cubic anharmonicity was obtained using the lattice Green's-function method, but these results rely on too many approximations to be a useful starting point for numerical simulations. In the work to be reported here, we introduce a static local distortion plus the rotating wave approximation to obtain analytical solutions for odd- and even-parity intrinsic localized modes with unrestricted cubic and quartic anharmonicities. Our findings are contrasted with those previously found for asymmetric envelope solitons using the continuum approximation.[13,14]

In Sec. II, we outline a general numerical solution of the nonlinear equations of motion for stationary and moving intrinsic localized modes where the rotating wave approximation is used to remove high-frequency harmonics. The amplitudes and velocities of the particles in the localized mode are found as a function of the anharmonic coefficients in the potential. In Sec. III, these amplitudes and velocities are used as initial conditions in simulations to compare the analytical and simulated local mode frequencies and to test the stability as a function of the anharmonic parameters. We identify the restricted anharmonicity region of the asymmetric envelope soliton obtained in the continuum approximation and contrast that with the unrestricted region of the local mode case. The frequencies and wave vectors of the moving modes are determined by numerically fitting the simulated displacement versus time curves and then compared to analytical values. The conclusions are presented in Sec. IV.

II. SOLUTION OF THE EQUATIONS OF MOTION

We consider a perfect one-dimensional (1D) monoatomic lattice in which each particle of mass m interacts only with its nearest neighbors through a potential that includes cubic and quartic nonlinearity. The equation of motion for the particle at the nth site is then

$$m\frac{d^2u_n}{dt^2}=K_2(u_{n+1}+u_{n-1}-2u_n)+K_3[(u_{n+1}-u_n)^2-(u_{n-1}-u_n)^2]+K_4[(u_{n+1}-u_n)^3+(u_{n-1}-u_n)^3]\,, \quad (1)$$

where K_2, K_3, and K_4 are harmonic, cubic, and quartic force constants, respectively, that are derived from the anharmonic potential. Anticipating the possibility of moving anharmonic modes, we seek a solution of the form

$$u_n=\alpha[\xi_n(t)+\phi_n(t)\cos(kna+\omega t)]\ , \tag{2}$$

where α is the maximum amplitude, a the lattice spacing, and $\cos(kna+\omega t)$ is a left moving carrier wave with wave vector k and frequency ω describing the localized mode. For a stationary mode ϕ_n, the vibrational envelope, and ξ_n, the static displacement, are independent of time, while for the moving mode case, $\phi_n(t)$ and $\xi_n(t)$ are slowly varying with time compared to the vibrational frequency. Next insert Eq. (2) into Eq. (1). Using the rotating wave approximation to remove high-frequency harmonics and the slowly varying time dependence of the envelope and static displacement terms to eliminate their second time derivatives, we obtain three coupled equations. To satisfy for all time the solution represented by Eq. (2), the coefficients of both the in-phase and out-of-phase oscillatory terms as well as those of the static displacement must independently sum to zero. Equating the coefficients of the sine terms gives

$$\begin{aligned}8\left[\frac{\omega}{\omega_m}\right]\left[\frac{d\phi_n}{dt}\right]=\omega_m\sin(ka)(&\phi_{n+1}\{1+\tfrac{3}{4}\Lambda[\phi_{n+1}^2-2\phi_{n+1}\phi_n\cos(ka)+\phi_n^2]+2\Gamma(\xi_{n+1}-\xi_n)+3\Lambda(\xi_{n+1}-\xi_n)^2\}\\&-\phi_{n-1}\{1+\tfrac{3}{4}\Lambda[\phi_n^2-2\phi_{n-1}\phi_n\cos(ka)+\phi_{n-1}^2]\\&+2\Gamma(\xi_n-\xi_{n-1})+3\Lambda(\xi_n-\xi_{n-1})^2\})\ ,\end{aligned} \tag{3}$$

the cosine terms,

$$\begin{aligned}4\left[\frac{\omega}{\omega_m}\right]^2\phi_n=&[\phi_n-\phi_{n+1}\cos(ka)]\{1+\tfrac{3}{4}\Lambda[\phi_{n+1}^2-2\phi_{n+1}\phi_n\cos(ka)+\phi_n^2]+2\Gamma(\xi_{n+1}-\xi_n)+3\Lambda(\xi_{n+1}-\xi_n)^2\}\\&+[\phi_n-\phi_{n-1}\cos(ka)]\{1+\tfrac{3}{4}\Lambda[\phi_n^2-2\phi_{n-1}\phi_n\cos(ka)+\phi_{n-1}^2]\\&+2\Gamma(\xi_n-\xi_{n-1})+3\Lambda(\xi_n-\xi_{n-1})^2\}\ ,\end{aligned} \tag{4}$$

and the static displacement terms,

$$\begin{aligned}&\Lambda(\xi_{n+1}-\xi_n)^3+\Gamma(\xi_{n+1}-\xi_n)^2+(\xi_{n+1}-\xi_n)\{1+\tfrac{3}{2}\Lambda[\phi_{n+1}^2-2\phi_{n+1}\phi_n\cos(ka)+\phi_n^2]\}+\tfrac{1}{2}\Gamma[\phi_{n+1}^2-2\phi_{n+1}\phi_n\cos(ka)+\phi_n^2]\\&\quad=\Lambda(\xi_n-\xi_{n-1})^3+\Gamma(\xi_n-\xi_{n-1})^2+(\xi_n-\xi_{n-1})\{1+\tfrac{3}{2}\Lambda[\phi_n^2-2\phi_{n-1}\phi_n\cos(ka)+\phi_{n-1}^2]\}\\&\qquad+\tfrac{1}{2}\Gamma[\phi_n^2-2\phi_{n-1}\phi_n\cos(ka)+\phi_{n-1}^2]\ ,\end{aligned} \tag{5}$$

where ω_m is the maximum plane-wave frequency, $\Gamma=K_3\alpha/K_2$, and $\Lambda=K_4\alpha^2/K_2$. Equation (5) must be satisfied at each lattice site, therefore each side is independently equal to a constant of motion. The anharmonic localized modes we seek are characterized by exponential decays of both the vibrational amplitude, ϕ_n and the relative distortion, $(\xi_{n+1}-\xi_n)$, therefore all the terms in Eq. (5) rapidly approach zero far from the mode center. The value of the constant must then be zero for a localized mode solution, and we may write

$$\begin{aligned}&\Lambda(\xi_n-\xi_{n-1})^3+\Gamma(\xi_n-\xi_{n-1})^2+(\xi_n-\xi_{n-1})\{1+\tfrac{3}{2}\Lambda[\phi_n^2-2\phi_{n-1}\phi_n\cos(ka)+\phi_{n-1}^2]\}\\&\qquad+\tfrac{1}{2}\Gamma[\phi_n^2-2\phi_{n-1}\phi_n\cos(ka)+\phi_{n-1}^2]=0\ .\end{aligned} \tag{6}$$

To proceed in our analytical solution, we assume an exponential decay of the vibrational amplitudes starting with the first neighbor.[5] A better solution can be obtained by beginning the exponential decay farther from the mode center, but this generates more equations and variables without significantly improving the accuracy. With this approximation, the odd-parity mode has the form

$$\begin{aligned}&\phi_0=1\ ,\quad \phi_n=\phi_{-n}=(-1)^n\phi_1 e^{-(n-1)qa}\quad (n>0)\ ,\\&\xi_0=0\ ,\quad \xi_n=-\xi_{-n}\ ,\end{aligned} \tag{7}$$

and the even mode is represented by

$$\begin{aligned}&\phi_0=1\ ,\quad \phi_{-1}=-1\ ,\\&\phi_n=-\phi_{-n-1}=(-1)^n\phi_1 e^{-(n-1)qa}\quad (n>0)\ ,\\&\xi_n=-\xi_{-n-1}\ .\end{aligned} \tag{8}$$

Note that the factors of $(-1)^n$ in the expression for ϕ_n indicate that we are measuring the wave vector from the zone boundary. For the odd mode, substitution of Eq. (7) into Eqs. (4) and (6) yields six coupled nonlinear equations which are numerically solved for the variables $\{\omega/\omega_m,\phi_1,e^{-qa},\xi_1,\xi_2-\xi_1,\xi_3-\xi_2\}$ for given values of the wave vector ka and the dimensionless anharmonicity parameters, Γ and Λ.[18] Similarly for the even mode, substitution of Eq. (8) into Eqs. (4) and (6) yields seven coupled

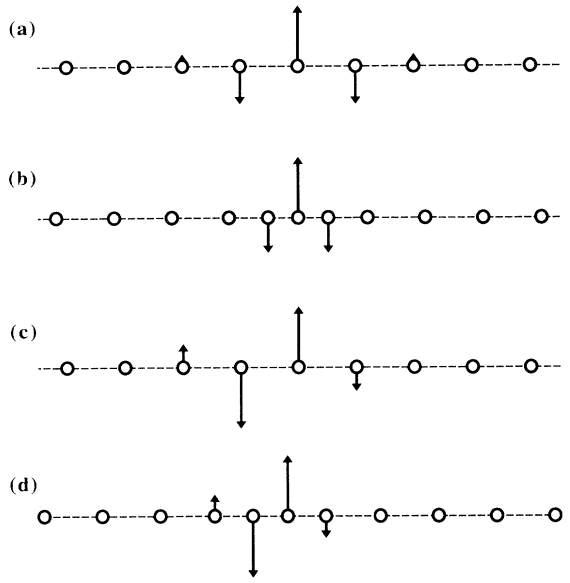

FIG. 1. Vibrational amplitudes and static displacement for odd and even intrinsic localized modes. The odd mode parameters are (a) $\Lambda=1.6$, $\Gamma=0.0$ and (b) $\Lambda=1.6$, $\Gamma=2.4$ with a maximum vibrational amplitude of 0.4 and a maximum static displacement of 0.32. The lattice parameter is 1. The even-mode parameters are (c) $\Lambda=0.9$, $\Gamma=0.0$ and (d) $\Lambda=0.9$, $\Gamma=1.2$ with a maximum vibrational amplitude of 0.3 and a maximum static displacement of 0.18.

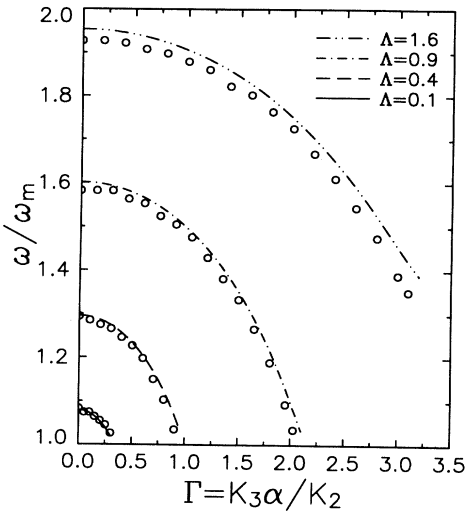

FIG. 2. Frequencies of stationary even parity modes as a function of the cubic anharmonicity Γ. The simulation and analytic results are represented by open circles and lines, respectively, for several values of the quartic anharmonicity Λ.

equations which are numerically solved for the variables $\{\omega/\omega_m,\phi_1,e^{-qa},\xi_1,\xi_2-\xi_1,\xi_3-\xi_2,\xi_4-\xi_3\}$. The remaining distortions, $\xi_{n+1}-\xi_n$, are then obtained from Eq. (6) for $n>3$ and $n>4$ for the odd and even modes, respectively, while the initial values of $d\phi_n/dt$ are calculated using Eq. (3).

The eigenvectors obtained using the procedure outlined above are shown in Fig. 1 for stationary odd and even modes with frequencies that are approximately 1.4 times the maximum frequency of the plane-wave spectrum. The vibrational amplitudes are drawn as vectors perpendicular to the axis of motion to distinguish them from the static displacement due to the cubic anharmonicity, and the sizes of the displacements relative to the lattice constant are exaggerated for clarity (see figure caption). As the cubic anharmonicity is increased from zero in Figs. 1(a) and 1(c) to significant positive values in Figs. 1(b) and 1(d) for the odd and even mode, respectively, the dominant effect is a compression about the center; conversely, lattices with negative cubic anharmonicity would exhibit a rarefaction. There is also a slight increase in the localization with the increased cubic anharmonicity, but this effect is small for the values of the quartic anharmonicity corresponding to these particular initial conditions.

III. COMPUTER SIMULATIONS

A. Stationary localized modes

Eigenvectors obtained by numerically solving the equations of motion such as those in Fig. 1 are used as initial conditions in a simulation program[8] which numerically integrates the equations of motions in a 1D monoatomic lattice with 512 sites and free end conditions. The lattice spacing, harmonic force constant, and mass are all set to unity, and the simulations are typically at least one hundred periods of the maximum frequency plane wave in order to observe the long term stability. Note that cubic anharmonicity changes the eigenvector of a stationary odd mode from $(\ldots,-\phi_1,1,-\phi_1,\ldots)$ to $(\ldots,-\phi_1-\xi_1,1,-\phi_1+\xi_1,\ldots)$, where ϕ_1 approaches $\frac{1}{2}$ for large quartic anharmonicity and the nearest-neighbor static displacement ξ_1 can be greater than 1 for large cubic anharmonicity. Note that the static displacement can be even larger than the maximum vibrational amplitude. Sandusky, Page, and Schmidt have reported that the odd-parity mode is unstable to this particular distortion and tends to move from its initial position, while the even mode remains stationary under the same perturbation.[10] We find that even for the large distortions used here, it takes 10–30 periods before the odd mode moves from its initial position, while the stationary even mode is stable for at least hundreds of periods.

Figure 2 shows the simulation results for frequencies of stationary even modes as a function of the cubic anharmonicity Γ for several values of Λ, the quartic anharmonicity. These are plotted as open circles, while the predicted frequencies from the analytical solution of the equations of motion [Eqs. (4) and (6)] are represented by different lines. There is good agreement over the entire range of cubic anharmonicities. When the redshift[5] due to higher-order harmonics is taken into account, the analytical frequencies decrease and there is better agreement with the simulations. Fourier transforms of the simulated displacement versus time curves indicate that the amplitude of the third harmonic is less than 5% of the fundamental, while the amplitude of the second har-

monic is always completely negligible, even for the maximum value of the cubic anharmonicity shown here.

The results plotted in Fig. 2 also show that there is a limiting value of Γ for a given value of Λ. The boundary line identifying the region of stable localized modes is shown in Fig. 3. For small values of Λ, the vibrational frequency decreases with increasing Γ until it approaches the maximum frequency of the plane-wave spectrum. The localized mode is then observed to rapidly decay into plane waves and therefore no longer represents a stable vibrational configuration. This condition, $(\omega/\omega_m)=1$, may be substituted into the equations of motion to obtain a stability curve in (Γ,Λ) space, which is plotted as the solid line label "b" in Fig. 3. This curve defines the minimum Λ value needed to support intrinsic localized modes for a given value of Γ. For larger values of Γ, the instability in the simulations occurs at frequencies above the maximum plane-wave frequency. An examination of the analytical solution shows that this different type of instability occurs due to the increase in localization with increasing Γ. This localization cannot increase beyond the vibrational amplitudes for the triatomic molecule limit, namely $(-\frac{1}{2},1,-\frac{1}{2})$, that exists for the odd mode in lattices with only positive quartic anharmonicity.[4] This localized eigenvector is substituted into the equations of motion to obtain a second instability curve, which is plottted as the dashed curve labeled "a" in Fig. 3.

There is now some value in contrasting our local mode results with the earlier work by Flytzanis *et al.* on asymmetric envelope solitons within the continuum approximation.[14] The asymmetric envelope soliton solutions described there have effective widths of at least 13.5 lattice sites, so to make a comparison, we solve the equations of motion for an intrinsic localized mode of the same width. This solution is plotted as the dotted curve labeled "c" in Fig. 3, and the area labeled "d" then defines that region where the continuum approximation is valid. This represents only a small fraction of the area supporting stable intrinsic localized modes, therefore the local mode solutions reported here cover a much larger region of physical space than those obtained using the continuum approximation.

B. Dispersion of moving localized modes

The initial amplitudes and velocities for nonzero wave vectors are calculated using the same method as for stationary modes. The displacements at three lattice sites are plotted as a function of time in Fig. 4 to show the static displacement and vibrational amplitude as the model propagates through the lattice. Consider the effect of the static displacement on the particle at the $n=10$ site in the figure. Initially, at small times, sites to the right of the mode are displaced to the left. Later as the mode moves through the tenth lattice site, this displacement goes to zero and then changes sign at larger times after the mode has moved past this lattice site. The group velocity of this particular moving excitation is approximately 15% of the lattice sound velocity. Note that there is a small increase in the static displacement at the $n=10$ site after a time corresponding to three periods of the maximum plane-wave frequency. This is caused by a small-amplitude, supersonic pulse that propagates in both directions from the local mode at the start of the simulation and eventually reaches the free ends of the lattice. This pulse may be a long-wavelength acoustic kink soliton that is also a solution of these equations of motion.[15]

Studies of moving asymmetric envelope solitons in the

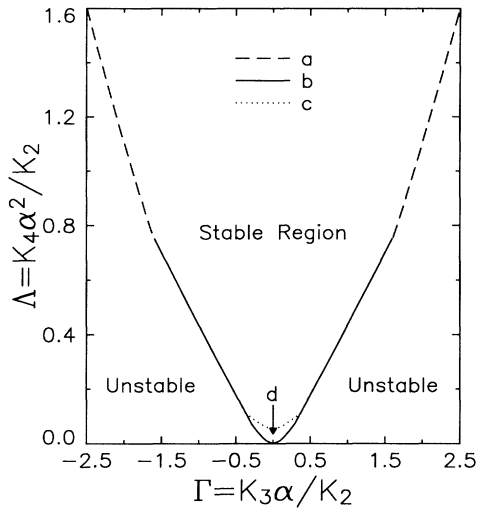

FIG. 3. Habitat of intrinsic localized modes in the space spanned by the cubic and quartic anharmonicities. Curves (a) and (b) represent boundaries where the modes become unstable due to the localization limit and the decay into plane waves, respectively. Area (d), lying between curves (b) and (c), designates the region of the continuum approximation as described in the text.

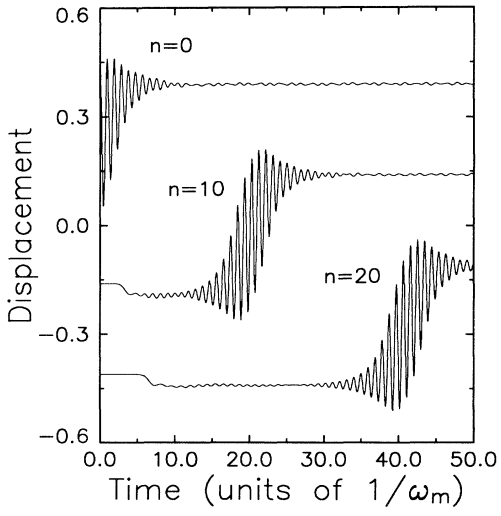

FIG. 4. Displacement versus time of a moving localized mode. The response at three equally spaced lattice sites shows the motion of an intrinsic localized mode characterized by the parameters, $\Lambda=0.4$, $\Gamma=0.8$, and $ka=0.3$. The three curves are displaced vertically by 0.25 units for clarity.

continuum approximation have shown that the solution is composed of the sum of two terms.[14] A cosine term modulated by a hyperbolic secant describes the high-frequency vibrations, while the static displacement is represented by a hyperbolic tangent function. However the local modes studied here are not well characterized by these functions, and in fact, the offsets can only be fit to a hyperbolic tangent if this function is raised to a large power. Since we have not characterized the static displacement around these localized modes with a single mathematical function, we quantitatively describe their properties by transforming to coordinates that depend on the difference of the displacements:[17]

$$w_n = u_{n+1} - u_n \ . \tag{9}$$

This transformation reverses the vibrational parity, so that modes that had even parity in u space now have odd-parity in w space and vice versa. In addition, the static component now decrease exponentially with increasing distance from the center. The simulated displacement versus time curves are then numerically fit using the function

$$w_n = \alpha[\zeta_n(t) + \phi_n(t)\cos(kna + \omega t)] \ , \tag{10}$$

where $\zeta_n(t)$ and $\phi_n(t)$ are now both approximated by Gaussian functions.[8] Earlier work on systems without cubic anharmonicity has shown that in order to determine the parameters of the carrier wave, there is some flexibility in choosing the functional form of the envelope of the moving localized mode.

The results plotted in Fig. 5 are for moving localized modes characterized by a single value of the wave vector that is used to calculate the initial displacements and velocities. The magnitude of the wave vector is $ka = 0.1$, which corresponds to moving localized modes with group velocities that are approximately 5% of the speed of sound in the monoatomic chain. The simulation frequencies, represented by the open circles, are in close agreement with the frequencies that are predicted by the analytic solutions of the equations of motion, which are plotted as lines for several values of the quartic anharmonicity. Note that this figure represents only a cross section of the space spanned by the parameters ka, Λ, and Γ and is only a small portion of the region where stable moving localized modes exist.

Figure 6 presents another way of demonstrating the simulation results. It shows the normalized frequency versus the wave vector at a particular plane crossing the Λ axis for several values of the cubic anharmonicity. The agreement between simulated and analytical frequencies is very good for small values of the wave vector and group velocity, but the simulation frequencies begin to decrease more rapidly at larger values. This occurs because the initial displacements and velocities are not exact eigenvectors, so the mode loses amplitude and energy as the relative displacements adjust to the correct configuration. The simulation data therefore correspond to smaller values of the cubic and quartic anharmonicity and are shifted downwards relative to the predicted values. The absence of simulation results in the lower right-hand corner of Fig. 6 represents the region where simulations produce modes that either decay into plane waves or slow down too rapidly to be characterized by a single wave vector. The top curve, corresponding to $\Gamma = 1.8$, represents the maximum cubic anharmonicity where stationary localized modes are stable for this particular Λ value. Note that the agreement between the simulation and analytic results is better at smaller wave vectors and higher frequencies because the effect of the second derivatives that were removed from the equation of motion is minimized and the exponential approximation of the eigenvector in Eqs. (7) and (8) is more accurate.

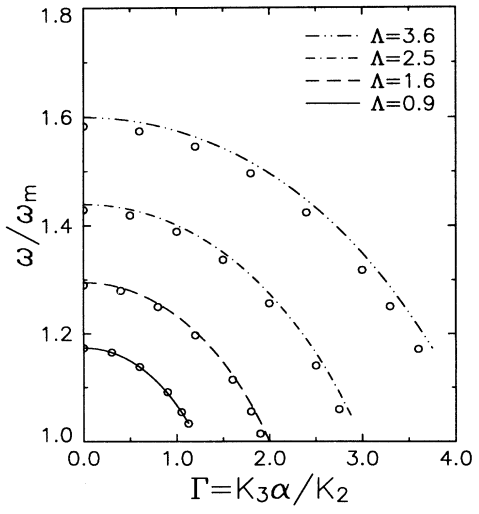

FIG. 5. Frequencies of moving localized modes as a function of Γ for several values of Λ. Simulation and analytical results are represented by open circles and lines, respectively, for a constant wave vector, $ka = 0.1$.

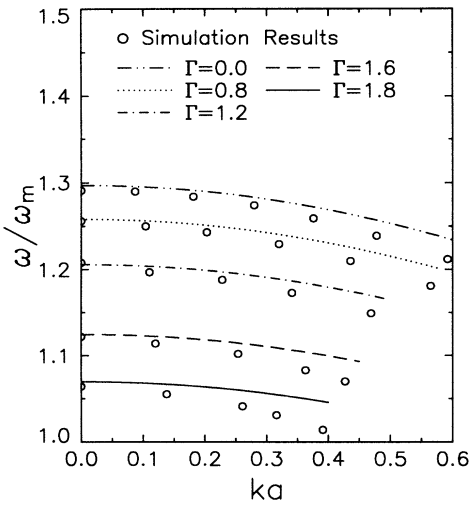

FIG. 6. Moving localized mode dispersion curves for diferent values of Γ. Simulation and analytical results are represented by open circles and lines, respectively, for $\Lambda = 1.6$.

IV. CONCLUSION

The intrinsic localized modes described here for a lattice with cubic and hard quartic nonlinearity in the nearest-neighbor provide examples of anharmonic vibrations that stabilize local static distortions. The excitation of such modes can produce either lattice expansion or contraction, depending on the sign of the cubic anharmonicity. The only restrictions on the relative sizes of the anharmonicities are that the frequency of the localized mode must be above the maximum frequency of the plane-wave spectrum and that the localization cannot increase beyond the limiting value of three and four sites for the odd- and even-parity mode, respectively. We have demonstrated that the eigenvectors found here are accurate in the limit of large amplitude and small width, in contrast with the asymmetric envelope soliton solutions obtained using the continuum approximation. Simulations are used to test the eigenvectors derived from the analytical solution of the equation of motion, and there is very good agreement over the entire range of cubic anharmonicities supporting intrinsic localized modes for any given value of the quartic anharmonicity. Finally, the dispersion curve has been found for moving localized modes in the presence of cubic anharmonicity, and again there is good agreement between simulation and analytical results.

ACKNOWLEDGMENTS

This work was supported by the NSF Grant No. DMR-89-18894 and the ARO Grant No. DAAL03-92-G-0369. Computing facilities were provided in part by the Cornell-IBM Joint Study on Computing for Scientific Research and in part by the MRL Central Facilities supported by the NSF under Award No. DMR-9121654. In addition, S.R.B. received partial support from AT&T Bell Laboratories.

[1]A. J. Sievers and S. Takeno, Phys. Rev. Lett. **61**, 970 (1988).
[2]S. Takeno and A. J. Sievers, Solid State Commun. **67**, 1023 (1988).
[3]S. Takeno *et al.*, Prog. Theor. Phys. Suppl. **94**, 242 (1988).
[4]J. B. Page, Phys. Rev. B **41**, 7835 (1990).
[5]S. R. Bickham and A. J. Sievers, Phys. Rev. B **43**, 2339 (1991)
[6]V. B. Burlakov *et al.*, Phys. Lett. A **147**, 130 (1990); Pis'ma Zh. Eksp. Teor. Fiz. **51**, 481 (1990) [JETP Lett. **51**, 544 (1990)].
[7]S. Takeno and J. Hori, J. Phys. Soc. Jpn. **59**, 3037 (1990).
[8]S. R. Bickham, A. J. Sievers, and S. Takeno, Phys. Rev. B **45**, 10 344 (1992).
[9]S. Takeno, J. Phys. Soc. Jpn. **59**, 1571 (1990).
[10]K. W. Sandusky, J. B. Page, and K. E. Schmidt, Phys. Rev. B **46**, 6161 (1992).
[11]E. Fermi, J. Pasta, and S. Ulam, *Collected Papers of Enrico Fermi* (University of Chicago Press, Chicago, 1965), p. 978.
[12]V. M. Burlakov *et al.*, Solid State Commun. **74**, 326 (1990); Phys. Rev. B **42**, 4921 (1990).
[13]A. M. Kosevich and A. S. Kovalev, Zh. Eksp. Teor. Fiz. **67**, 1793 (1974) [Sov. Phys. JETP **40**, 891 (1975)].
[14]N. Flytzanis *et al.*, J. Phys C: Solid State Phys. **18**, 4603 (1985).
[15]V. M. Burlakov and S. A. Kiselev, Zh. Eksp. Teor. Fiz. **99**, 1526 (1991) [Sov. Phys. JETP **72**, 854 (1991)].
[16]S. Takeno and J. Hori, J. Phys. Soc. Jpn. **60**, 947 (1991).
[17]M. Toda, in *Theory of Nonlinear Lattices,* edited by M. Cardona, P. Fulde, and H.-J. Queisser, Springer Series in Solid State Sciences Vol. 20 (Springer, Berlin, 1981).
[18]The systems of nonlinear equations are solved using an IMSL Math and Statistics Library routine that employs the Levenberg-Marquardt algorithm and a finite-difference approximation to the Jacobian.